Available online at www.sciencedirect.com
ScienceDirect
Journal of Power Sources 161 (2006) 301–307
JOURNAL OF POWER SOURCES
www.elsevier.com/locate/jpowsour

NiO–YSZ cermets supported low temperature solid oxide fuel cells

Xinge Zhang *, Mark Robertson, Cyrille Decès-Petit, Yongsong Xie, Rob Hui, Sing Yick, Edward Styles, Justin Roller, Olivera Kesler, Radenka Maric, Dave Ghosh

Institute for Fuel Cell Innovation, National Research Council Canada, 3250 East Mall, Vancouver, BC, Canada V6T 1W5

Received 1 March 2006; received in revised form 22 March 2006; accepted 28 March 2006
Available online 6 May 2006

Abstract

Solid oxide fuel cells with thin electrolyte of two types, $Sm_{0.2}Ce_{0.8}O_{1.9}$ (SDC) (15 μm) single-layer and 8 mol% Yttria stabilized zirconia (YSZ) (5 μm) + SDC (15 μm) bi-layer on NiO–YSZ cermet substrates were fabricated by screen printing and co-firing. A $Sm_{0.5}Sr_{0.5}CoO_3$ cathode was printed, and in situ sintered during a cell performance test. The SDC single-layer electrolyte cell showed high electrochemical performance at low temperature, with a 1180 mW cm^{-2} peak power density at 650 °C. The YSZ + SDC bi-layer electrolyte cell generated 340 mW cm^{-2} peak power density at 650 °C, and showed good performance at 700–800 °C, with an open circuit voltage close to theoretical value. Many high Zr-content micro-islands were found on the SDC electrolyte surface prior to the cathode preparation. The influence of co-firing temperature and thin film preparation methods on the Zr-islands' appearance was investigated.

Keywords: SOFC; Low temperature; SDC; YSZ; Bi-layer electrolyte

1. Introduction

During the last decade, Nickel-Yttria Stabilized Zirconia (Ni-YSZ) anode supported solid oxide fuel cells (SOFCs) with thin-film electrolytes have been widely adopted by industrial pioneers and research groups in the world. Encouraging performance in the intermediate temperature range (700–800 °C) with thin-film YSZ electrolytes has been achieved [1]. However, a high degradation rate in cell performance at the stack level has been observed, which is related to thermally activated material degradation, in particular, high temperature corrosion of steel interconnects [2,3]. Extensive R&D efforts are continuing to decrease cell operating temperature below 600 °C.

The practical operating temperature of SOFCs is mainly determined by the conductivity and thickness of the electrolyte. Doped ceria is a promising option for an electrolyte material for low temperature use. It has an ionic conductivity that is 2–3 times higher than that of YSZ, and better compatibility with Co-containing electrodes. Its thermal expansion coefficient (12.5×10^{-6} K^{-1}) is also more compatible with that of the Ni-cermet substrate and commercial ferritic stainless steel interconnect, compared with YSZ. The maximum power density of 0.25 W cm^{-2} at 550 °C with an anode-supported thin ceria based electrolyte cell has been reported [4,5]. The main disadvantage of a ceria-based electrolyte is that it becomes a mixed conductor under anodic conditions, which causes a cell voltage loss and fuel efficiency loss due to internal shorting. Chemical and mechanical stability, thermal cycle capability and redox tolerance as well are other concerns for long-term service.

To lower manufacturing cost, efforts have been underway to bring proven microelectronics manufacturing technology to SOFCs, such as Tape casting of cermet substrates, Screen printing of functional layers, and Co-firing of cell components (TSC technology in short). Interest is also growing in applying metal supported cell structures [6,7].

In this study, TSC technology was used to fabricate NiO–YSZ cermet supported cells with thin electrolytes of two types, $Sm_{0.2}Ce_{0.8}O_{1.9}$ (SDC) (15 μm) single-layer and 8 mol% Yttria stabilized zirconia (YSZ) (5 μm) + SDC (15 μm) bi-layer, It has been found that the SDC single-layer electrolyte cell shows very high performance at temperatures below 650 °C while the YSZ + SDC bi-layer electrolyte cell shows good performance over 700 °C, with open circuit voltage close to theoretical value. The elemental analysis reveals many high-Zr-content

* Corresponding author. Tel.: +1 604 221 3077; fax: +1 604 221 3088.
E-mail address: xinge.zhang@nrc.gc.ca (X. Zhang).

0378-7753/$ – see front matter © 2006 Elsevier B.V. All rights reserved.
doi:10.1016/j.jpowsour.2006.03.057

Table 1
Chemical composition, properties, supplier of starting materials

Material	Composition	Properties	Supplier
Cathode	$Sm_{0.5}Sr_{0.5}CoO_3$ (SSCo)	D50: 0.80 μm Surface area: 5.16 $m^2\ g^{-1}$	Praxair
Electrolyte	$(SmO_{1.5})_{0.2}(CeO_2)_{0.8}$ (SDC)	D50: 0.40 μm Surface area: 7.08 $m^2\ g^{-1}$	Praxair
	8Y (YSZ) $(YO_{1.5})_{0.16}(ZrO_2)_{0.84}$	D50: 0.26 μm Surface area: 13.0 $m^2\ g^{-1}$	Tosoh
Anode	$(SmO_{1.5})_{0.2}(CeO_2)_{0.8}$ (SDC)	D50: 0.40 μm Surface area: 7.08 $m^2\ g^{-1}$	Praxair
	8Y (YSZ)	D50: 0.260 μm Surface area: 13.0 $m^2\ g^{-1}$	Tosoh
	NiO type F	D50: 1.0 μm Surface area: 4.0 $m^2\ g^{-1}$	Novamet
Cermet substrate	NiO-standard	D50: 16.0 μm Surface area: <1 $m^2\ g^{-1}$	
	8YS (YSZ)	D50: 0.520 μm Surface area: 6.2 $m^2\ g^{-1}$	Tosoh

Table 2
Organic chemicals for tape casting and screen-printing

	Chemicals	Function	Supplier
Tape casting	Polyvinyl butyral, B-76	Binder	Richard E. Mistler, Inc.
	Emphos 236	Dispersant	Richard E. Mistler, Inc.
	Santiciser-160, Ucon-50	Plasticizer	Richard E. Mistler, Inc.
	Toluene, MIBK, Ethanol	Solvent	Alfa Aesar
Screen printing	B-76, Ethyl cellulose	Binder	Richard E. Mistler, Inc. Acros Organics
	Menhaden fish Oil (MFO Z-3), Sorbitan monooleate(SM)	Dispersant	Richard E. Mistler, Inc. GEOspecialty chemicals
	Butyl acetate, isopropanol, Butanol, α-Terpineol	Solvent	Alfa Aesar

micro-islands on the surface of the thin SDC layer and at the cross-section of the SDC electrolyte. The influence of co-firing temperature and thin-film preparation methods on the appearance of the Zr-islands has been investigated.

2. Experimental procedure

2.1. Starting materials and cell fabrication

Table 1 lists the starting ceramic powder materials used in this study. The organic materials used for tape casting and screen-printing are listed in Table 2. All the materials for cell fabrication are commercially obtained.

Fig. 1 shows the schematic for cell structure, which consists of cermet substrate, anode layer, electrolyte and cathode. The cell fabrication route consists of tape-casting the substrate, screen-printing the anode and then the electrolyte on the substrate, high temperature co-firing, printing the cathode and firing the cathode during the cell electrochemical test. Table 3 lists the cell materials, thicknesses, and processing conditions. Different anode materials were used for the two types of cells, according to the electrolyte materials used: Ni-SDC anode for the SDC electrolyte and Ni-YSZ anode for the YSZ + SDC electrolyte. 57 wt.% NiO + 43 wt.% YSZ powder mixture was chosen for both NiO–YSZ cermet substrate and NiO–YSZ anode. For NiO-SDC anode the composition was changed to 53 wt.% NiO + 47 wt.% SDC in order to yield the same Ni volume percent (41 vol%) as in the NiO–YSZ anode and substrate according to the density difference between YSZ and SDC.

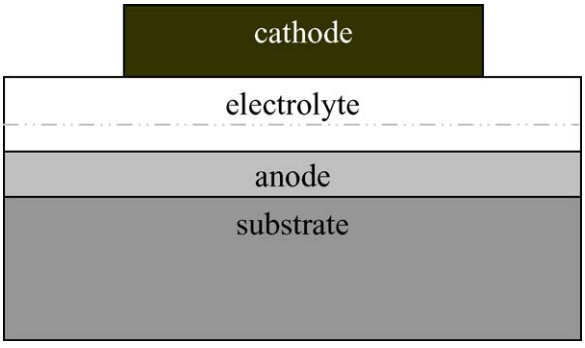

Fig. 1. Schematic of cell structure.

Table 3
Cell materials, thicknesses, and processing conditions

Cell type	SDC		YSZ + SDC		Condition	
	Material	Thick (μm)	Material	Thick (μm)	Temp. (°C)	Time (h)
Cathode	SSCo	20–30	SSCo	20–30	900	2
Electrolyte	SDC	15	SDC	15		
			YSZ	5	1400	2
Anode	Ni-SDC	15	Ni-YSZ	15		
Substrate	Ni-YSZ	600	Ni-YSZ	600		

Table 4
Physical characterization for cells fired at 1400 °C for 2 h

Cell Type	SDC single layer electrolyte	YSZ + SDC bi-layer electrolyte
Electrolyte appearance	Transparent	Transparent
Cell shrinkage (%)	15.6	15.8
Cell density (g cm^{-3})	5.25	5.26
Substrate porosity (%)	17.2	17.0
13.8 kPa helium leakage rate (ml min^{-1} cm^{-2})	Not detectable	Not detectable

2.2. Cell characterization

The results of the physical characterizations of the fired cells are summarized in Table 4. It was found that the SDC electrolyte could be sintered to fully dense at 1400 °C, while the YSZ electrolyte could be fully sintered at 1350 °C. The well-sintered electrolytes appear transparent, and allow no detectable helium gas cross leakage at 13.8 kPa (about 2 psi), indicating that the electrolyte layers were fully dense. After the electrolyte quality characterizations, each cell was characterized by an Archimedes density measurement to obtain the cermet substrate density and porosity. The measured cell densities are 5.25 g cm^{-3} on average. It indicates 17.2% porosity in the NiO–YSZ cermet substrate based on the cermet substrate composition of 57 wt.% NiO. The substrate porosity will be increased to approximately 30% porosity after NiO reduction to Ni.

The cell used in this study is 15 mm in diameter, with cermet substrate thickness of approximately 0.6 mm. $Sm_{0.5}Sr_{0.5}O_3$ (SSCo) cathode of 0.40–0.41 cm^2 was applied at the centre of each cell by stencil printing, and dried at 100 °C for 1 h. The cathode thickness is approximately 20–30 μm after in situ sintering.

Fig. 2 shows a schematic setup for button cell electrochemical tests. A split-tube furnace (Thermcraft incorporated) was used for cell temperature control. The thermal couple for furnace temperature control was located nearby the cell at the anode side. The cells were mounted for electrochemical testing at the end of an alumina tube, and sealed with a commercial sealing paste (ceramabond #552). A thin layer $Sm_{0.5}Sr_{0.5}O_3$ (SSCo) paste was applied to the Pt mesh at the cathode side to create a good contact between the cathode and the cathode current collector (Pt mesh) in the testing apparatus. A constant spring loaded force was applied to the cathode air supply alumina tube, of approximately 1.0 kgf according to the deformation of loading springs. The cell was heated up to 900 °C at a ramp rate of 300 °C h^{-1}, and held for 2 h for cathode in situ sintering. The temperature was then decreased to 700 °C for anode reduction and cell electrochemical measurements. Ambient air was introduced at a flow rate of 100 ml min^{-1} to the cathode side. Hydrogen or a H_2:N_2 = 1:1 mixture at the same total flow rate was first passed through a bubbler-type humidifier at room temperature, corresponding to a 3% H_2O content, and then introduced to the anode side during the test.

Electrochemical measurements were performed at the temperatures ranging from 700 to 450 °C for the SDC single-layer electrolyte cells and 750 to 600 °C for SDC + YSZ bi-layer electrolyte cells under ambient pressure. Cell performances were measured with a Multi-channel Potentiostat/Galvanostat (Solartron 1480 8 channel multi-stat) with a computer interface and Corr-view software. The I–V curves and power curves

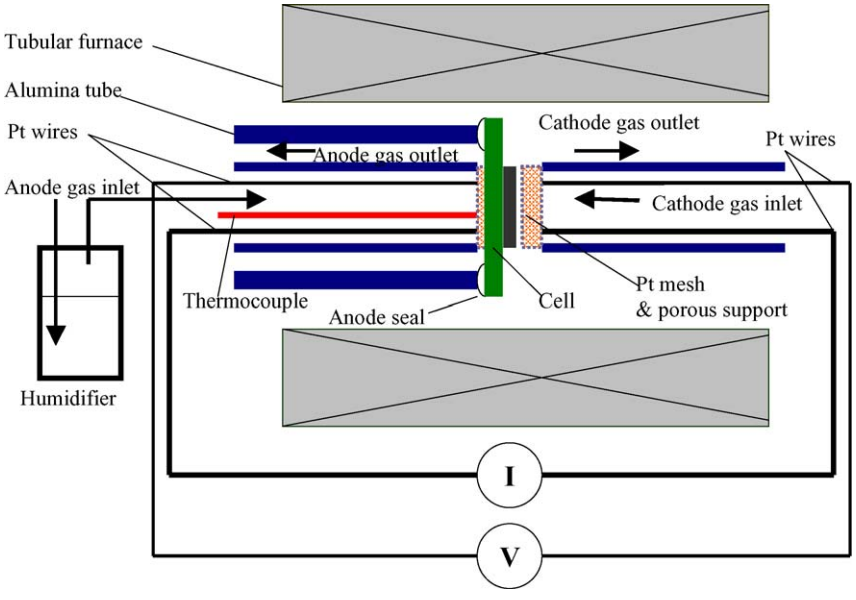

Fig. 2. Schematic setup for button cell test.

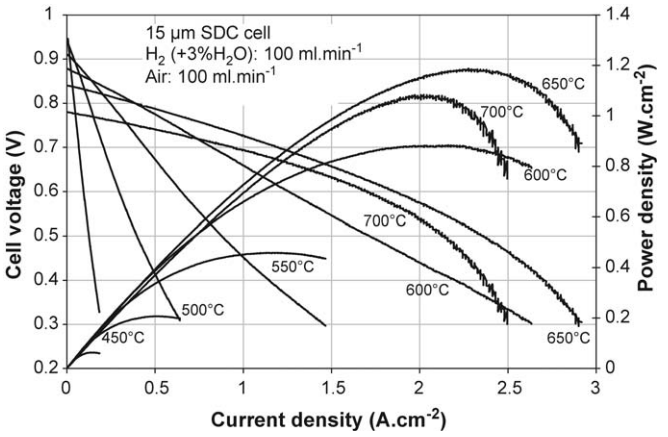

Fig. 3. I–V power curves of a15 μm SDC single layer electrolyte cell co-fired with anode at 1400 °C, and SSCo cathode sintered at 900 °C, tested at different operating temperatures.

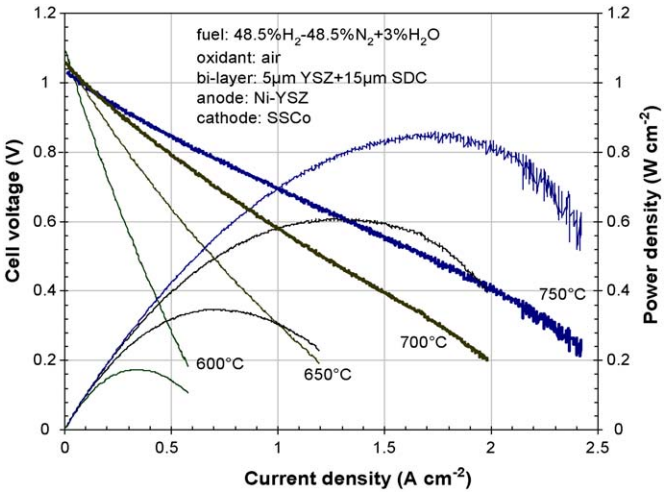

Fig. 4. I–V power curves of a cell with 5 μm YSZ + 15 μm SDC bi-layer electrolyte co-fired with Ni-YSZ anode at 1400 °C, and SSCo cathode sintered at 900 °C, tested at different operating temperatures.

were obtained using linear sweep voltammetry at a sweep rate of 4 mV s^{-1} from OCV to 0.3 V. The morphologies of the tested cells were observed using a scanning electron microscope (SEM, Hitachi S-3500N) coupled with energy dispersive spectrometry (EDS) and X-ray diffraction techniques for element analysis.

3. Results and discussion

3.1. Cell electrochemical performance

Fig. 3 shows the performance of a single-layer SDC electrolyte cell. It can be seen that the maximum power densities of the SDC electrolyte cell reached 1187 mW cm^{-2} at 650 °C, 0.884 mW at 600 °C, and 459 mW cm^{-2} at 550 °C. These values are higher than reported data in the literature with similar cell configurations in this temperature range [4,5,7,8]. The main differences between the present cells and the cells reported in the literature are the in situ sintering of the cathode, and a slightly thinner SDC electrolyte layer in this study.

The performance of a cell with YSZ + SDC bi-layer electrolyte is presented in Fig. 4. Although the performance is reasonably high at an elevated temperature range, the low temperature performance is much lower than that of the SDC cell. The maximum power density is only approximately 340 mW cm^{-2} at 650 °C. It can be seen that the OCV of this bi-layer electrolyte cell is much higher than that of the SDC single layer electrolyte cell, and is very close to the theoretical OCV value in the tested temperature range. This indicates that the YSZ layer plays the role in obstructing the electronic conductivity in the bi-layer electrolyte and preventing the internal shorting of the cell. Furthermore, the dense YSZ layer prevents the anodic reducing atmosphere from directly contacting the SDC electrolyte layer. Therefore, the electronic conductivity in the SDC electrolyte is prevented. The low cell performance of the bi-layer electrolyte cell likely results from the combination of a low ionic conductivity of the additional YSZ layer, a detrimental inter-reaction between the SDC and YSZ layer, and a lower anode performance of Ni-YSZ in comparison with Ni-SDC. Fig. 5 shows the area specific resistances (ASR) of the 15 μm thick SDC and 5 μm thick YSZ at different temperatures, which was generated from the reported conductivity of SDC [9] and YSZ [10]. It can be seen that the ASR value of 15 μm thick SDC is almost equal to the 5 μm thick YSZ in the listed temperature range, indicating that the ohmic loss of the bi-layer electrolyte cell will be twice higher than the single layer SDC electrolyte cell. However, the calculated electrolyte ohmic loss at 650 °C is only 50 mV at 1 A cm^{-2}, which is insufficient to explain the low performance of bi-layer electrolyte cell at this temperature. Being aware of that SDC has a higher ionic conductivity and catalytic activity than YSZ, it is rational that Ni-SDC anode in the single layer SDC electrolyte cell may slightly perform better than that of Ni-YSZ anode in the bi-layer cell. The difference of anode gas composition will also have influence. But the authors believe that the main contributor to the low performance of the bi-layer electrolyte cell is a detrimental interaction between YSZ and SDC.

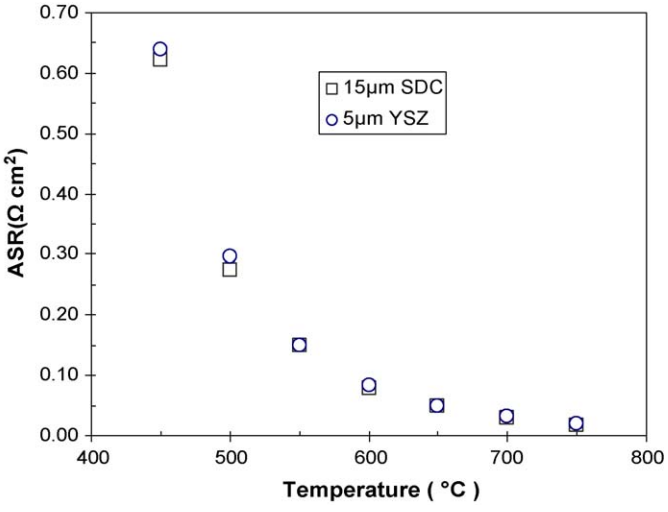

Fig. 5. Area specific resistances (ASR) of 15 μm thick SDC and 5 μm thick YSZ at different temperatures.

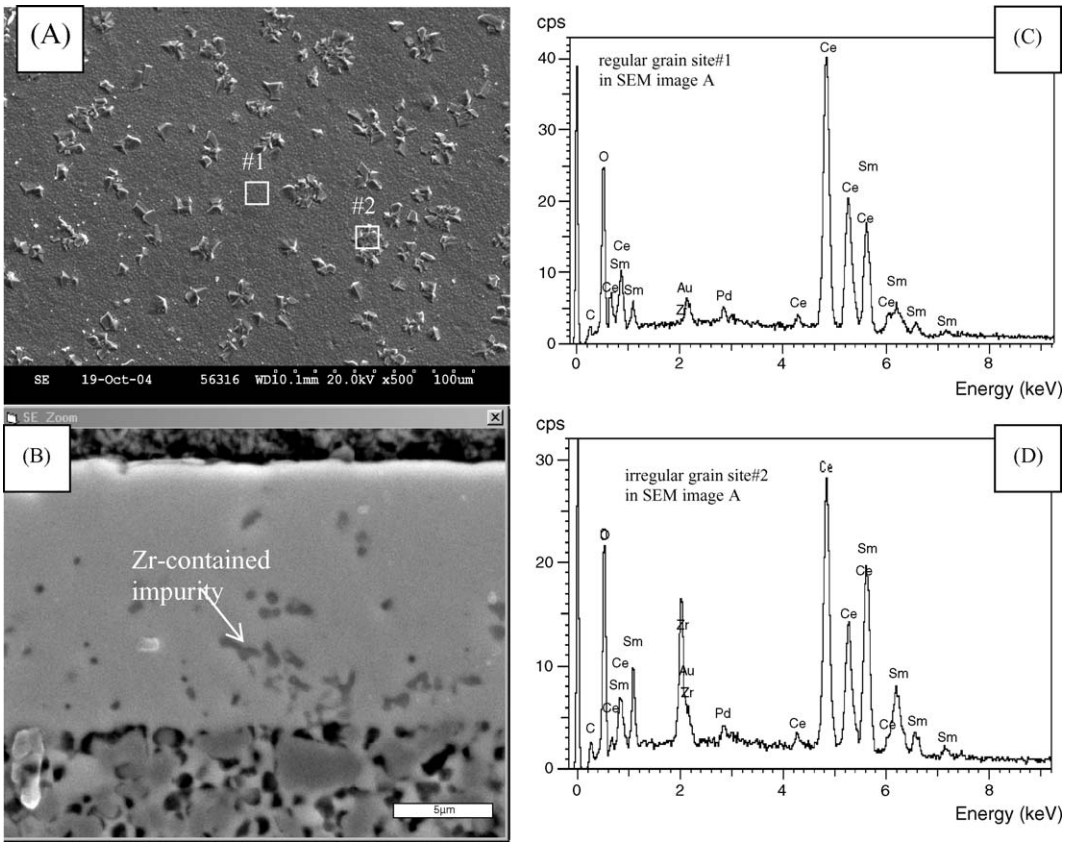

Fig. 6. Microstructure and EDS analysis of the tested thin SDC cell. (A) Plan view of SDC cell electrolyte surface without cathode; (B). Cross-section of the tested SDC cell (polished); (C) EDS analysis result of SDC electrolyte at a regular grain; (D) EDS analysis result of SDC electrolyte at an irregular grain.

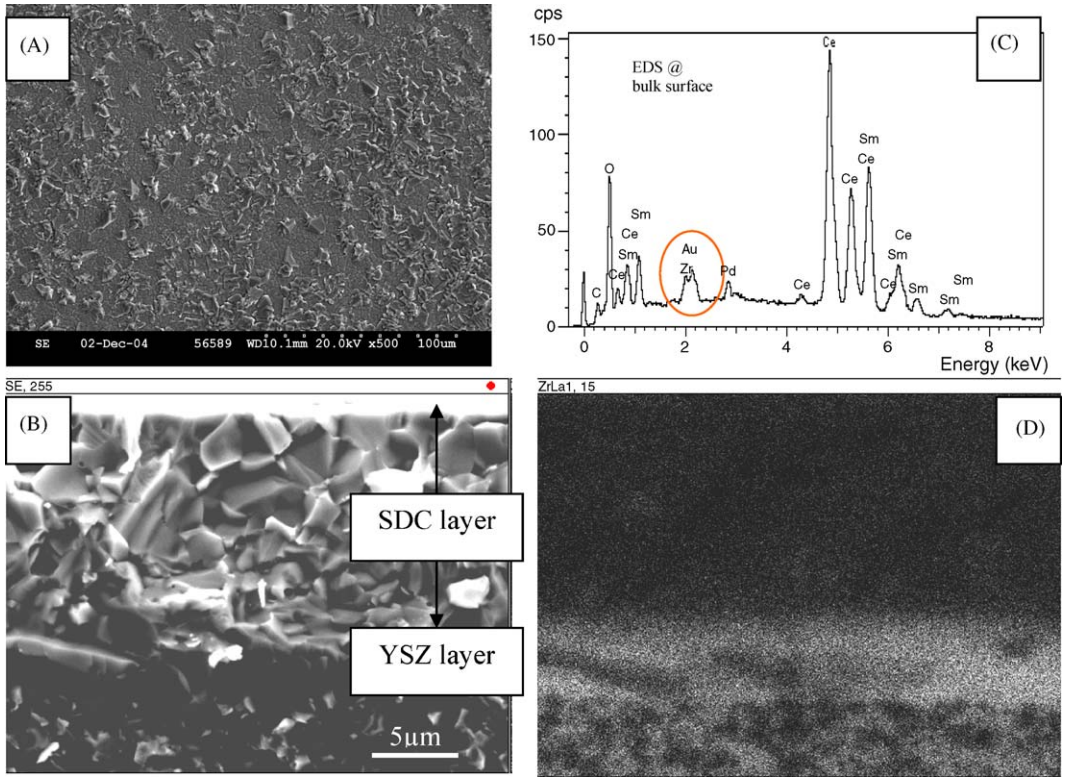

Fig. 7. Microstructure and EDS analysis of the tested thin YSZ + SDC cell. (A) Plan view of YSZ + SDC cell electrolyte surface without cathode; (B) Cross-section of the tested YSZ + SDC cell (not polished); (C) EDS analysis result of the SDC bulk surface; (D) Zirconium mapping of the cross-section of the YSZ + SDC cell.

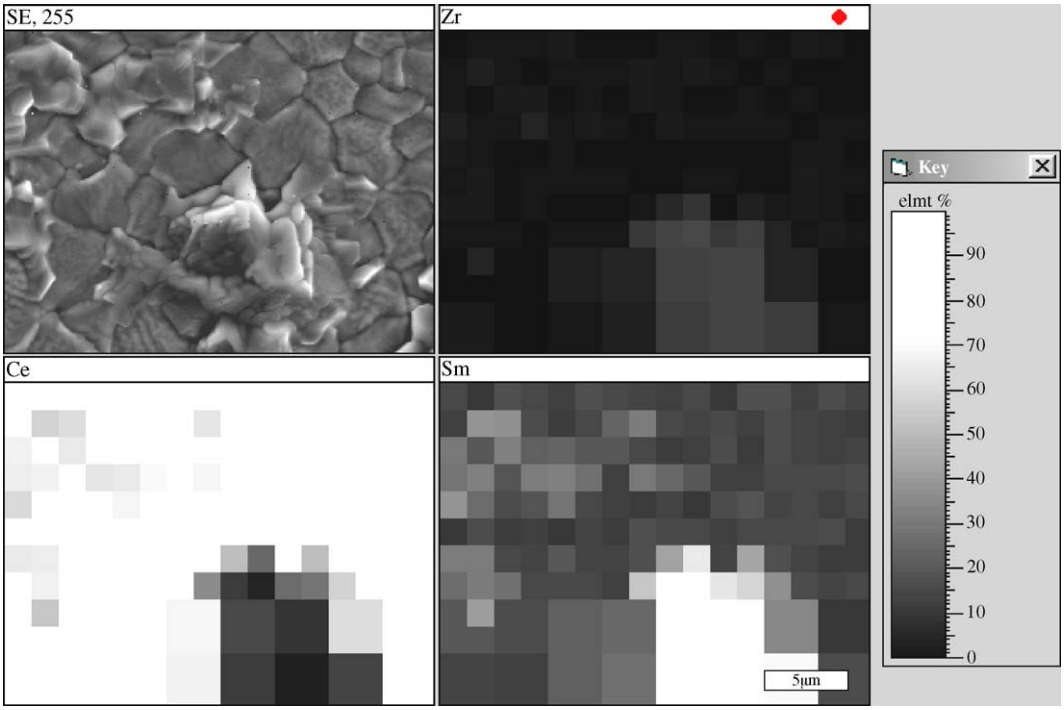

Fig. 8. X-ray elemental mapping of an irregular grain area.

3.2. Cell microstructure characterization and EDS analysis

Figs. 6 and 7 show plan and cross-section views of the tested cells, including EDS analyses of the electrolytes. Many irregular grains on the SDC electrolyte surface were observed after the 1400 °C–2 h co-firing and prior to cathode deposition. EDS analysis results (Fig. 6D) show that the irregular grains have a high Zr content, and have the appearance of micro-islands, so they are referred to as Zr-micro-islands in this work. The cross-section of the SDC electrolyte after sample polishing also reveals a dark pore-like inclusions (Fig. 6B), which in fact are Zr-content inclusions verified by EDS analysis. There are many more of these Zr-micro-islands in the YSZ + SDC bi-layer electrolyte cell (Fig. 7A) than in the SDC single-layer electrolyte cell (Fig. 6A). Fig. 7D shows the Zirconium element mapping of the cross section of the YSZ + SDC bi-layer electrolyte cell as mechanically fractured sample without polishing (Fig. 7B). It proves that the YSZ layer (approximately 5 μm) applied adjacent to the anode has not chemically mixed with the sequential SDC layer after high temperature co-firing. It is hard to see from Fig. 7D that the existence of Zr (if any) present in the cross section of the SDC layer, which could be attributed to this SEM sample without polishing.

3.3. Zr-micro-islands

EDS analysis was used to examine one of the irregular grain areas at higher resolution. Fig. 8 shows the results. It can be seen that the irregular grain shows not only a high Zr-content, but also an enriched Sm content, while the Ce content is substantially decreased. This result suggests that Zr has replaced the Ce site in the normal SDC lattice, or that a second Sm-rich phase containing Zr separates from the SDC phase. High Sm content in the irregular grain indicates that Sm has a higher solubility in the new phase. Furthermore, since the grain size of the Zr-island is larger than that of the normal SDC grains, this second phase likely also has a higher vapour pressure or lower melting point, a faster grain growth rate, and higher sinterability than that of normal SDC during the cell co-firing.

The Zr-micro-islands are potentially detrimental to the cell performance. Tsoga et al. [11] reported that the Zr–Ce–Gd–Y–O composite phase exhibits a conductivity two orders of magnitude lower than that of either GDC or YSZ. Table 5 lists their conductivity data, recorded at 800 °C. Since Sm-doped ceria and Gd-doped ceria have very similar conductivities, it is likely that the Zr micro-islands observed in this work may also consist of a very low conductivity phase, based on the analyzed compo-

Table 5
Ionic conductivity (σ_{ion}) and electronic conductivity (σ_n^o) of YSZ, GDC and their mixed composites at 800 °C [9]

Material	Nominal composition	σ_{ion} (S cm^{-1})	σ_n^o (S cm^{-1})
YSZ	$Zr_{0.85}Y_{0.15}O_{1.93}$	0.054	7.29×10^{-13}
GDC	$Ce_{0.80}Gd_{0.20}O_{1.90}$	0.087	8.18×10^{-6}
Reaction product	$Ce_{0.37}Zr_{0.38}$ $Gd_{0.18}Y_{0.07}O_{1.87}$	0.00125	3.99×10^{-6}
Interlayer	$Ce_{0.43}Zr_{0.43}$ $Gd_{0.10}Y_{0.04}O_{1.93}$	0.00603	3.88×10^{-6}

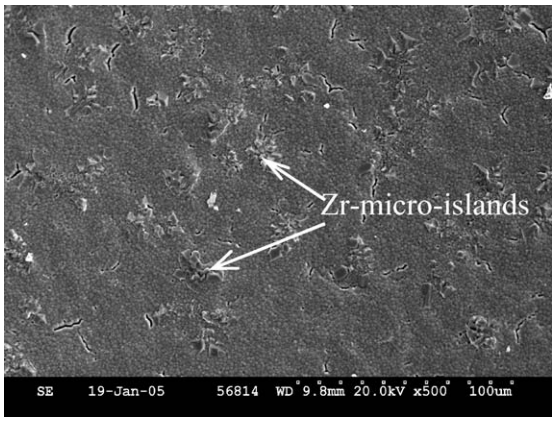

Fig. 9. SEM image of a cell with spin-coated SDC electrolyte fired at 1400 °C.

sitions, and their similarity with the compositions studied by Tsoga et al.

The formation mechanism of the Zr-micro-islands is not clear. The SDC electrolyte paste was investigated and no any Zr contamination was found. The influence of sintering temperature was also studied, and it was found that lower sintering temperatures produced fewer obvious irregular grains. Cells co-fired at 1250 °C did not show any irregular grains, which suggests either that no Zr migration (and Zr-micro-island formation) occurred, or that the grains have not grown large enough to be detected, due to the slow grain growth rates at the low sintering temperatures. No clear location showing a high Zr content on the cells sintered at 1250 °C was found. Spin coating of the electrolyte layers was conducted to determine whether the formation of Zr-islands results from potential inter-contamination during screen-printing. Similar irregular grains on the SDC surface were found after firing at 1400 °C (Fig. 9). The formation of Zr-micro-islands is therefore likely related to Zr migration from the NiO–YSZ substrate during the co-firing process.

4. Conclusions

SDC single-layer electrolyte cells and YSZ + SDC bi-layer electrolyte cells supported by Ni-YSZ substrates were prepared by tape casting, screen printing, and co-firing technology. Using in situ sintered SSC cathodes, high performance of over 1180 mW cm^{-2} peak power density at 650 °C was obtained from the SDC electrolyte cells. The bi-layer cells did show higher OCV values, but their performances were much lower than those of the SDC cells at low operating temperatures. Zr-micro-island formation on the SDC electrolyte was observed, with compositions indicating that an interaction between YSZ and SDC took place during the high-temperature co-firing of the cells.

Acknowledgement

The authors would like to thank the National Research Council of Canada for supporting the low temperature SOFC project.

References

[1] S. de Souza, S.J. Visco, L.C. De Jonghe, Solid State Ionics 98 (1997) 57–61.
[2] Z. Yang, K.S. Weil, D.M. Paxton, J.W. Stevenson, J. Electrochem. Soc. 150 (2003) A1188–A1201.
[3] W.Z. Zhu, S.C. Deevi, Mater. Res. Bull. 38 (2003) 957–972.
[4] C. Xia, W. Rauch, F. Chen, M. Liu, Solid State Ionics 149 (2002) 11–19.
[5] S. Zha, W. Rauch, M. Liu, Solid State Ionics 166 (2004) 241–250.
[6] Schiller, G., Henne, R., Lang, M., Schaper, S., Development of Metallic Substrate Supported Thin-Film SOFC by Applying Plasma Spay Techniques, in: Proc. SOFC VI, Electrochem. Soc., 1999, pp. 893–903.
[7] N.P. Brandon, A. Blake, D. Corcoran, D. Cumming, A. Duckett, K. El-Koury, D. Haigh, C. Kidd, R. Leah, G. Lewis, C. Matthews, N. Maynard, N. Oishi, T. McColm, R. Trezona, A. Selcuk, M. Schmidt, L. Verdugo, J. Fuel Cell Sci. Technol. 1 (2004) 61–65.
[8] S. Zha, A. Moore, H. Abernathy, M. Liu, J. Electrochem Soc. 151 (2004) A1128–A1133.
[9] V.V. Kharton, F.M.B. Marques, A. Atkinson, Solid State Ionics 174 (2004) 135–149.
[10] S.P.S. Badwal, Solid State Ionics 52 (1992) p23.
[11] A. Tsoga, A. Naoumidis, D. Stover, Solid State Ionics 135 (2000) 403–409.